RSC Advances

PAPER

View Article Online
View Journal | View Issue

Cite this: *RSC Adv.*, 2019, **9**, 3279

Pressure-induced effects in the inorganic halide perovskite $CsGeI_3$

Diwen Liu, [ac] Qiaohong Li, *[a] Huijuan Jing [ac] and Kechen Wu*[ab]

Perovskite photovoltaic materials are gaining significant attention due to their excellent photovoltaic properties. In this study, density functional theory calculations were performed to investigate the structure and electronic and optical properties of $CsGeI_3$ under hydrostatic strain. The results show that the band gap of $CsGeI_3$ can be tuned from 0.73 eV to 2.30 eV under different strain conditions. The results indicate that the change in the band gap under strain is likely to be determined by the Ge–I–Ge bond angle. Interestingly, the length of the short Ge–I bond remains unchanged, whereas that of the long Ge–I bond exhibits an evident increment with strain ranging from −4% to 4%. A suitable band gap (1.36 eV) of $CsGeI_3$ can be obtained under a strain of −1%. Both the calculated elastic constants and the phonon spectrum imply that this structure is stable under the abovementioned condition. Bandgap narrowing induces a red shift of the light absorption spectrum of $CsGeI_3$ by extending the onset light absorption edge. These results are important for understanding the effects of strain on the halide perovskites and guiding the experiments to improve the photovoltaic performance of the perovskite solar cells.

Received 14th December 2018
Accepted 8th January 2019

DOI: 10.1039/c8ra10251a

rsc.li/rsc-advances

1. Introduction

Methyl-ammonium lead iodide perovskite ($CH_3NH_3PbI_3$) has become a leading photovoltaic material because of its distinctive advantages including suitable band gap, strong and wide absorption range for visible light, and low manufacturing cost.[1–7] The power conversion efficiency (PCE) of these materials has increased with a surprising spurt from 3.8% in 2009 (ref. 8) to 23.3% in 2018.[9] This rapid progress was achieved within eight years as a result of intensive investigations involving the composition of the perovskite material to optimize its electronic and optical properties through elemental substitution.[10,11] The replacement of Pb by the element Sn was proposed to be more environmentally friendly. However, the photovoltaic performance of the Sn-based perovskite $CH_3NH_3SnI_3$ was much lower than those of Pb-based perovskite materials.[2,12] According to the Shockley–Queisser theory, the PCE of $CH_3NH_3PbI_3$ perovskite solar cells was predicted to reach up to 33% when the band gap of the perovskite material was tuned to the range of 1.2–1.4 eV.[13] To further improve the PCE of perovskites to approach the ideal bandgap value, an effective way is to narrow the bandgap of the perovskite materials; this will broaden their light absorption in the visible light region.

In recent years, many studies have been carried out using strain engineering, which makes it possible to enhance particular properties of a material. Strain engineering, as an effective approach, has been reported to adjust the structures and electronic properties of organic–inorganic halide perovskites and provide further understanding of the structure–property relationships.[14–32] The effects of pressure on the structure and band gap of $CsGeBr_3$ and $CsGeCl_3$ were also studied.[33,34] Inorganic halide perovskite $CsGeI_3$ is stable up to 350 °C, with devices recording efficiency to only 0.2%.[35] The photovoltaic performance of $CsGeI_3$ can be further improved by narrowing the band gap of $CsGeI_3$ in the range of 1.2–1.4 eV. To the best of our knowledge, to date, the geometric structure and the electronic and optical properties of $CsGeI_3$ under strain have not been reported.

In this study, first-principles calculations were performed to explore the geometric structure and electronic and optical properties of $CsGeI_3$ under different strain conditions. We investigated the band structure for $CsGeI_3$ by two different methods. The variation in the bandgap with the increasing and decreasing external strain was studied. The changes in the structural parameters were further analysed to better understand the electronic properties of $CsGeI_3$. The optical absorption of $CsGeI_3$ was further investigated under different strain conditions.

2. Computational methods

DFT calculations were performed using the Vienna ab initio simulation package (VASP) code[36] with the implemented

[a]State Key Laboratory of Structural Chemistry, Fujian Institute of Research on the Structure of Matter, Chinese Academy of Sciences, Fuzhou 350002, P. R. China. E-mail: lqh2382@fjirsm.ac.cn; wkc@fjirsm.ac.cn; Fax: +86 591 63173138

[b]Center for Advanced Marine Materials and Smart Sensors, Minjiang University, Fuzhou 350116, P. R. China

[c]University of Chinese Academy of Sciences, Beijing 100049, P. R. China

projector augmented-wave (PAW) method.[37] The generalized gradient approximation in the Perdew–Burke–Ernzerhof form (GGA-PBE)[38] was used to describe the exchange correlation for electrons. The van der Waals (vdW) correction was considered with the optB86b-vdW functional. The plane-wave energy cut-off was set to 500 eV for geometric optimization and electronic structure calculations. The geometric structure of $CsGeI_3$ was fully relaxed until the energy and force were converged to 1.0^{-5} eV and 0.01 eV $Å^{-1}$, respectively. Monkhorst–Pack *k*-mesh sampling of the Brillouin zone was performed using a $4 \times 4 \times 4$ grid for structural relaxation and an $8 \times 8 \times 8$ grid for optical properties. As is well-known, GGA-PBE provides an underestimated band gap of halide perovskites. To obtain an accurate description of the electronic structures, Heyd–Scuseria–Ernzerhof (HSE06) hybrid functional calculations were performed.[39,40] The exact Hartree–Fock exchange contribution for the hybrid functional was set to 60% for the $CsGeI_3$ perovskite to reproduce the experimental values. The hydrostatic strain has been simulated by simultaneously changing the lattice parameters *a*, *b*, and *c*, which are determined by the expression $a = a_0(1+\varepsilon)$, $b = b_0(1+\varepsilon)$, and $c = c_0(1+\varepsilon)$. Herein, a_0, b_0, c_0 are the corresponding lattice constants without strain, and the value ε increases and decreases in the step of $\pm 1\%$ until it reaches $\pm 4\%$.

3. Results and discussion

3.1 Geometric structure

The trigonal structure of $CsGeI_3$ is depicted in Fig. 1. Geometric optimization of the $CsGeI_3$ structure has been performed using different functionals to find out the functional that provides the best fit for the experiment. We considered four functionals *i.e.* GGA-PBE,[38] PBEsol,[41] vdW-DF,[42] and optB86b-vdW.[43] The results are summarized in Table 1. It can be seen that both the PBE and vdW-DF functionals overestimate the lattice constants and volumes. The variation between the theoretical lattice constants and the experimental data is less than 1% when the optB86b-vdW functional is employed.[44] PBEsol also offers similar results. If the lattice constants and volumes are considered, the optB86b-vdW functional yields the best results. Moreover, the calculated short and long Ge–I bond lengths are about 2.80 Å and 3.15 Å, which agree with experimental data of 2.75 Å and 3.26 Å, respectively.[44]

Table 1 Lattice constant and volume of $CsGeI_3$ with PBE and with various functionals compared with the corresponding experimental results

	a $Å^{-1}$	b $Å^{-1}$	c $Å^{-1}$	V $Å^{-3}$
PBE	8.53	8.53	10.90	686.01
PBEsol	8.27	8.27	10.26	607.93
vdW-DF	8.67	8.67	11.22	729.76
optB86b-vdW	8.33	8.33	10.41	625.82
Exp[a]	8.36	8.36	10.61	641.89

[a] From ref. 44.

For the halide perovskite $CsGeI_3$, by changing the lattice constant of the $CsGeI_3$ structure, the structure was optimized to obtain a series of changes of energies, volumes, Ge–I–Ge bond angles, and Ge–I bond lengths. The detailed changes of these structural parameters are displayed in Fig. 2. It can be seen that the effects of strain have great impacts on the energies, volumes, Ge–I–Ge bond angles, and Ge–I bond lengths. Whether it is compressive or tensile strain, the stability of the structure is less than that of $CsGeI_3$ without strain. Upon applying compressive (tensile) strain, the volume will decrease (increase). The Ge–I–Ge angles show a gradual reduction with the ε value ranging from -4% to 4%. The Ge–I bonds in $CsGeI_3$ are divided into two kinds of bonds: short and long bonds. As shown in Fig. 2(d), the length of the short Ge–I bond remains unchanged, whereas that of the long Ge–I bond exhibits an evident increment with the ε value ranging from -4% to 4%. The change in the Ge–I–Ge angles and Ge–I bond lengths would significantly influence the electronic structures of $CsGeI_3$.

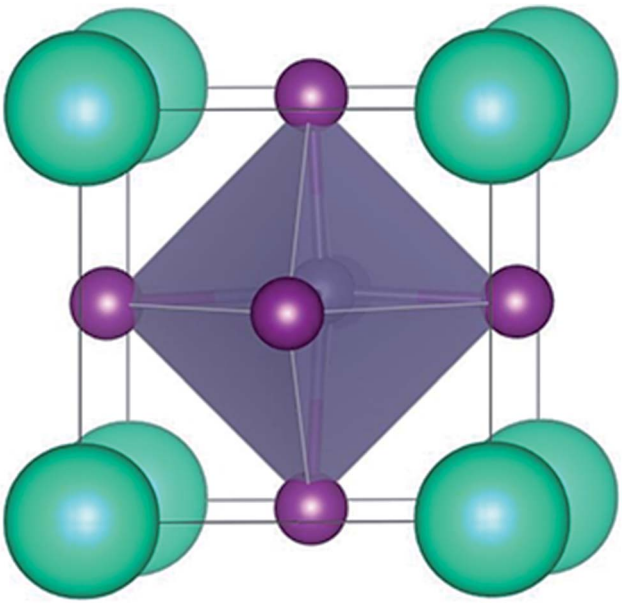

Fig. 1 The crystal structure of $CsGeI_3$.

3.2 Electronic properties

To better explore the electronic properties of $CsGeI_3$, we employed two DFT methods. The band gap of $CsGeI_3$ is found to be 0.68 eV by PBE calculation, which agrees well with other theoretical results.[45,46] However, this value is much smaller than the experimental results. To obtain more accurate band gap, we have used HSE06 calculation. The band structure of $CsGeI_3$ is shown in Fig. 3. It can be seen that $CsGeI_3$ is a direct bandgap semiconductor with a value of 1.56 eV, which is in good agreement with previous experimental results.[35,44] The density of states (DOS) and partial DOS of $CsGeI_3$ perovskite are presented in Fig. 3. Cs^+ does not contribute to the band edge states because the states of Cs^+ are far from the Fermi level. The valence band maximum (VBM) of $CsGeI_3$ is mainly contributed by the I-5p orbital, whereas the conduction band minimum (CBM) is dominated by the Ge-4p orbital.

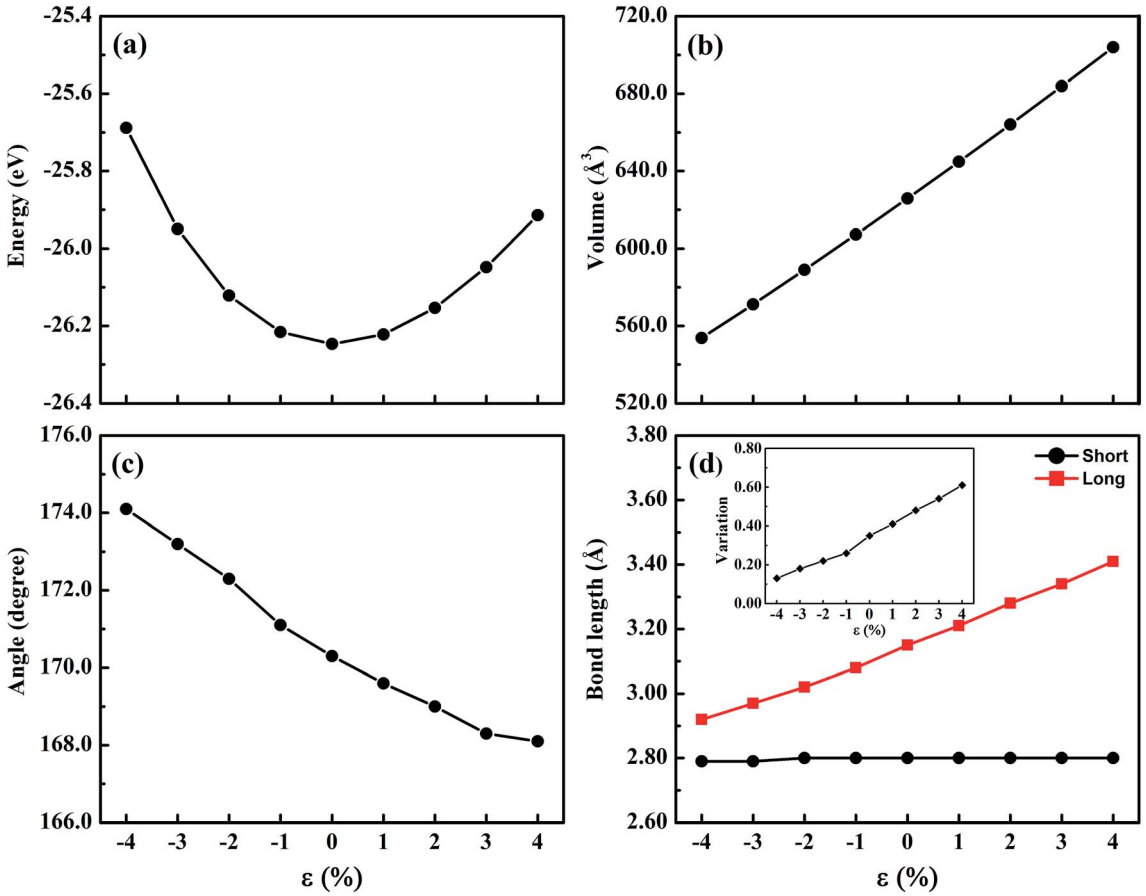

Fig. 2 The structural parameters of $CsGeI_3$ under different strain conditions. (a) The curve of energy. (b) The curve of volume. (c) The curve of the Ge–I–Ge angle. (d) The curve of the Ge–I bond length. The variation of the short and long Ge–I bond lengths is shown in the inset of (d).

The effects of strain on the band gap of $CsGeI_3$ were investigated. When strain was applied in the range from −4% to 4%, the band gaps of $CsGeI_3$ tuned from 0.73 to 2.30 eV. Interestingly, $CsGeI_3$ still remains a direct-bandgap semiconductor over the whole strain range. Both the CBM and VBM of $CsGeI_3$ decrease when strain is applied in the range from −4% to 4%.

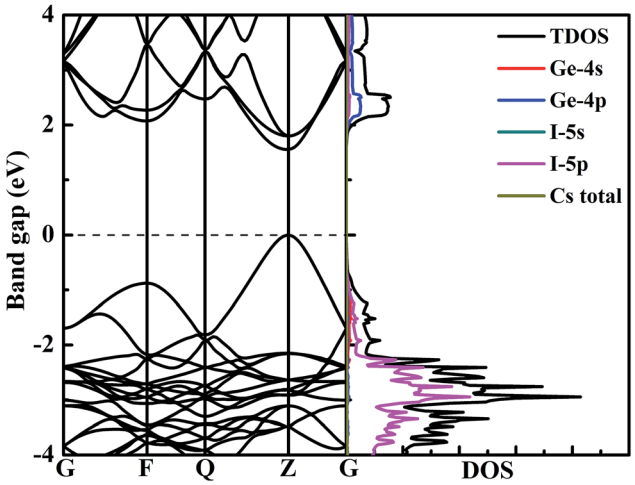

Fig. 3 The band structure and density of states of $CsGeI_3$ calculated at the HSE06 level.

The band gap of $CsGeI_3$ with $\varepsilon = -1\%$ is 1.36 eV, which is in the range of 1.3–1.4 eV. It indicates that this structure will have the best photovoltaic performance under this condition according to the Shockley–Queisser theory.[47] A suitable band gap can be obtained by applying a rather weak pressure (0.52 GPa). The band gaps of the $CsGeI_3$ structure calculated at the PBE level show trends similar to those calculated at the HSE06 level, as shown in Fig. 4(a). The relationships between stress and strain for $CsGeI_3$ under different conditions are shown in Fig. 4(b). It can be seen that the value of stress gradually decreases when ε increases from −4% to 4%.

It is important to understand the reasons for the change in the band gap of $CsGeI_3$ under strain. The response of the band gap under strain can be related with the geometry changes. A previous study has indicated that the electronic properties of hybrid perovskites are affected by structural distortion, and the main factor is the Pb–I–Pb bond angle.[48] The Ge–I–Ge bond angles of $CsGeI_3$ under different strain conditions are shown in Fig. 2(c). The smaller distortion of the Ge–I–Ge bond angle for $CsGeI_3$ ($\varepsilon = -4\%$) results in a smaller band gap of 0.73 eV when compared with that of $CsGeI_3$ (1.56 eV) without strain. However, the slightly greater distortion of the Ge–I–Ge bond angle for $CsGeI_3$ ($\varepsilon = 4\%$) results in a higher band gap of 2.30 eV when compared with that of $CsGeI_3$ without strain. It can be seen that the change in the Ge–I–Ge bond angles can provide an

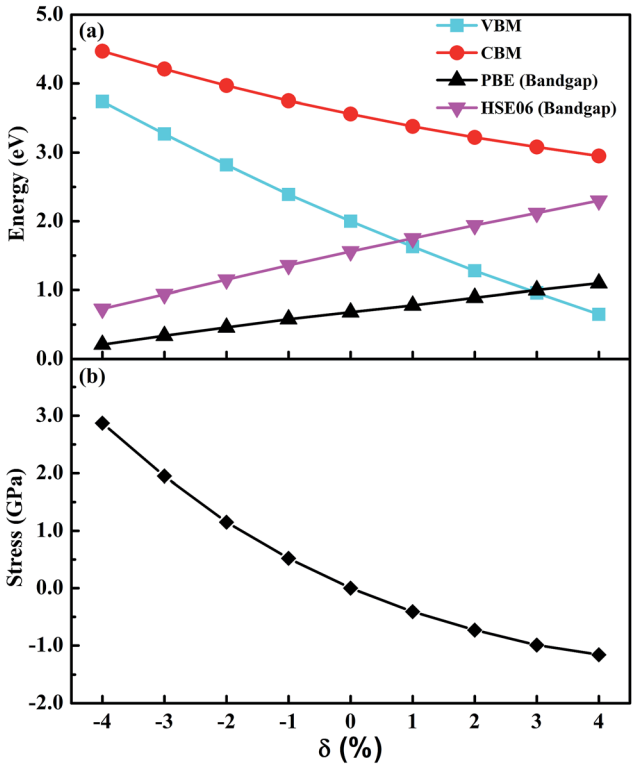

Fig. 4 (a) VBM, CBM, bandgap and (b) stress of $CsGeI_3$ as a function of strain.

explanation for the difference in the band gap of $CsGeI_3$ under different strain conditions.

We then mainly evaluated the stability of $CsGeI_3$ under a strain of −1%. The elastic constants are essential to predict the mechanical stability of a crystal. The well-known stability criteria for a trigonal crystal is given by $C_{11} - |C_{12}| > 0$, $(C_{11} + C_{12})C_{33} > 2C_{13}^2$, $(C_{11} - C_{12})C_{44} > 2C_{14}^2$.[49] The calculated elastic constants satisfy the stability criteria; this implies that this compound is mechanically stable. In addition, the phonon spectrum of this compound has been studied and is shown in Fig. 5. None of the imaginary phonon mode exists in the calculated phonon spectra; this suggested that this compound is kinetically stable. Based on the abovementioned stability study, i$CsGeI_3$ ($\varepsilon = -1\%$) can be obtained under proper experimental conditions.

To estimate the amount of charge transfer between atoms due to the hydrostatic strain, we have calculated the Bader charges of $CsGeI_3$ under different strain conditions. The results of the charge transfer are shown in Fig. 6. The Bader charges of Cs, Ge, and I ions fluctuate from 0.81 to 0.86e, 0.64 to 0.67e, and −0.48 to −0.51e, respectively. Compressive strain results in a decrease in the partial charges of Cs and Ge. On the contrary, tensile strain increases the values of the partial charges of Cs and Ge atoms. A similar change of the partial charges of I is also observed.

3.3 Optical properties

The investigation of the optical properties of materials is important to reveal the response of materials to light. Therefore,

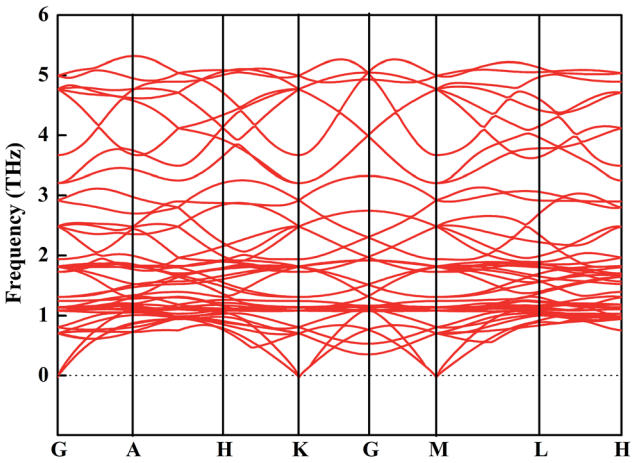

Fig. 5 Phonon spectrum of $CsGeI_3$ ($\varepsilon = -1\%$).

deep insights into the optical parameters are essential for the practical applications of materials in optoelectronic devices. To better understand the optical performance of $CsGeI_3$ under different strain conditions, we further calculated the optical absorption coefficients in the visible spectrum. The absorption coefficient $I(\omega)$ was calculated from the dielectric function as below:[50]

$$I(\omega) = \sqrt{2}\omega\left[\sqrt{\varepsilon_1(\omega)^2 + \varepsilon_2(\omega)^2} - \varepsilon_1(\omega)\right]^{1/2} \quad (1)$$

where $\varepsilon_1(\omega)$ and $\varepsilon_2(\omega)$ represent the real and imaginary parts of the dielectric function depending on the light frequency ω, respectively. The optical absorption spectra were obtained using the PBE functional with a scissor operator to obtain the band gap calculated at the HSE06 level. The calculated optical absorption spectrum of $CsGeI_3$ under different strain conditions is presented in Fig. 7. The calculated absorption spectra of $CsGeI_3$ without strain obtained in our study agrees well with the experimental result.[44] It can be clearly seen that the absorption edge shows a significant redshift when compressive strain is applied. When tensile strain is applied, the absorption edge shows a significant blueshift. The structures under compressive

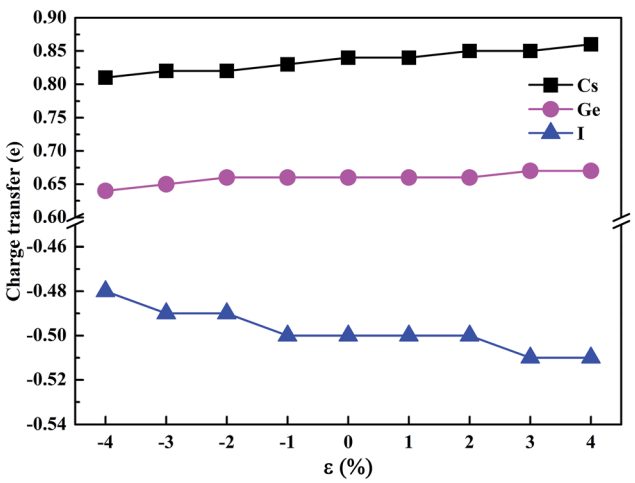

Fig. 6 The charge transfer of the Cs, Ge, and I atoms.

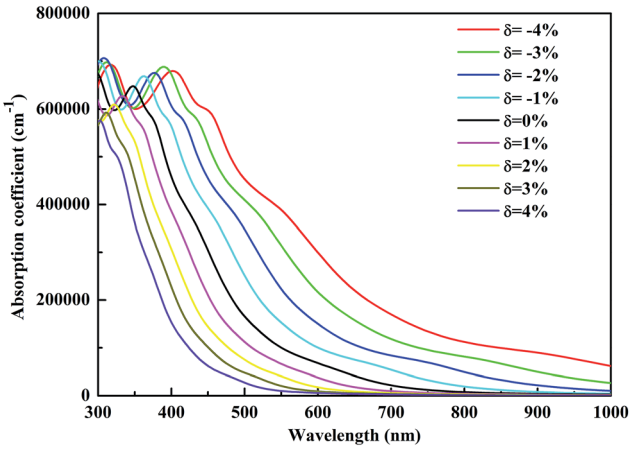

Fig. 7 Calculated optical absorption coefficients of $CsGeI_3$ under different strain conditions.

strains have a higher absorption strength in the visible light region than the unstressed structure. This situation is apparently the opposite for the structures under tensile strains. The strain-induced optical absorption variation of $CsGeI_3$ is well consistent with the predicted band gap.

4. Conclusion

In summary, we have systematically investigated the effects of strain on the structure, electronic and optical properties of $CsGeI_3$ using the first-principles calculations. Our results show that the band gap of $CsGeI_3$ can be tuned from 0.73 eV to 2.30 eV under different strain conditions. The results indicate that the change in the band gap under strain is likely to be determined by the Ge–I–Ge bond angle. The length of the short Ge–I bond remains unchanged, whereas that of the long Ge–I bond shows an evident increment with strain ranging from −4% to 4%. A suitable band gap (1.36 eV) is obtained upon applying a strain of −1%. Moreover, the $CsGeI_3$ structure is predicted to be stable under this condition. Bandgap narrowing induces the redshift of the light absorption spectrum of $CsGeI_3$ by extending the onset light absorption edge. Bandgap engineering by applying strain makes the halide perovskite $CsGeI_3$ achieve a suitable band gap and optical absorption, and thus, $CsGeI_3$ becomes a promising material for photovoltaic applications. Our results provide an efficient and clean approach to optimize the photovoltaic performance of the inorganic halide perovskite $CsGeI_3$.

Conflicts of interest

There are no conflicts to declare.

Acknowledgements

This work was supported by the National Science Foundation of China (No. 21673240) and the Foreign Cooperation Project of Fujian Province (No. 2017I0019).

References

1 W. Nie, H. Tsai, R. Asadpour, J.-C. Blancon, A. J. Neukirch, G. Gupta, J. J. Crochet, M. Chhowalla, S. Tretiak, M. A. Alam, H.-L. Wang and A. D. Mohite, *Science*, 2015, **347**, 522–525.
2 F. Hao, C. C. Stoumpos, D. H. Cao, R. P. H. Chang and M. G. Kanatzidis, *Nat. Photonics*, 2014, **8**, 489.
3 J. You, Z. Hong, Y. Yang, Q. Chen, M. Cai, T.-B. Song, C.-C. Chen, S. Lu, Y. Liu, H. Zhou and Y. Yang, *ACS Nano*, 2014, **8**, 1674–1680.
4 J. H. Noh, S. H. Im, J. H. Heo, T. N. Mandal and S. I. Seok, *Nano Lett.*, 2013, **13**, 1764–1769.
5 N. J. Jeon, J. H. Noh, W. S. Yang, Y. C. Kim, S. Ryu, J. Seo and S. I. Seok, *Nature*, 2015, **517**, 476–480.
6 H.-S. Kim, C.-R. Lee, J.-H. Im, K.-B. Lee, T. Moehl, A. Marchioro, S.-J. Moon, R. Humphry-Baker, J.-H. Yum, J. E. Moser, M. Grätzel and N.-G. Park, *Sci. Rep.*, 2012, **2**, 591.
7 D. Shi, V. Adinolfi, R. Comin, M. Yuan, E. Alarousu, A. Buin, Y. Chen, S. Hoogland, A. Rothenberger, K. Katsiev, Y. Losovyj, X. Zhang, P. A. Dowben, O. F. Mohammed, E. H. Sargent and O. M. Bakr, *Science*, 2015, **347**, 519–522.
8 A. Kojima, K. Teshima, Y. Shirai and T. Miyasaka, *J. Am. Chem. Soc.*, 2009, **131**, 6050–6051.
9 NREL, Best Research-Cell Efficiences chart, http://www.nrel.gov/pv/assets/images/efficiency-chart-20180716.jpg.
10 Y. Jiao, F. Ma, G. Gao, H. Wang, J. Bell, T. Frauenheim and A. Du, *RSC Adv.*, 2015, **5**, 82346–82350.
11 M. Lyu, J.-H. Yun, M. Cai, Y. Jiao, P. V. Bernhardt, M. Zhang, Q. Wang, A. Du, H. Wang, G. Liu and L. Wang, *Nano Res.*, 2016, **9**, 692–702.
12 N. K. Noel, S. D. Stranks, A. Abate, C. Wehrenfennig, S. Guarnera, A.-A. Haghighirad, A. Sadhanala, G. E. Eperon, S. K. Pathak, M. B. Johnston, A. Petrozza, L. M. Herz and H. J. Snaith, *Energy Environ. Sci.*, 2014, **7**, 3061–3068.
13 W. E. I. Sha, X. Ren, L. Chen and W. C. H. Choy, *Appl. Phys. Lett.*, 2015, **106**, 221104.
14 Y.-Q. Zhao, B. Liu, Z.-L. Yu, D. Cao and M.-Q. Cai, *Electrochim. Acta*, 2017, **247**, 891–898.
15 Y.-Q. Zhao, Q.-R. Ma, B. Liu, Z.-L. Yu and M.-Q. Cai, *Phys. Chem. Chem. Phys.*, 2018, **20**, 14718–14724.
16 Y. Nagaoka, K. Hills-Kimball, R. Tan, R. Li, Z. Wang and O. Chen, *Adv. Mater.*, 2017, **29**, 1606666.
17 A. Jaffe, Y. Lin, W. L. Mao and H. I. Karunadasa, *J. Am. Chem. Soc.*, 2017, **139**, 4330–4333.
18 Q. Li, S. Li, K. Wang, Z. Quan, Y. Meng and B. Zou, *J. Phys. Chem. Lett.*, 2017, **8**, 500–506.
19 P. Wang, J. Guan, D. T. K. Galeschuk, Y. Yao, C. F. He, S. Jiang, S. Zhang, Y. Liu, M. Jin, C. Jin and Y. Song, *J. Phys. Chem. Lett.*, 2017, **8**, 2119–2125.
20 L. Wang, K. Wang, G. Xiao, Q. Zeng and B. Zou, *J. Phys. Chem. Lett.*, 2016, **7**, 5273–5279.
21 L. Wang, K. Wang and B. Zou, *J. Phys. Chem. Lett.*, 2016, **7**, 2556–2562.

22 I. P. Swainson, M. G. Tucker, D. J. Wilson, B. Winkler and V. Milman, *Chem. Mater.*, 2007, **19**, 2401–2405.
23 A. Jaffe, Y. Lin, C. M. Beavers, J. Voss, W. L. Mao and H. I. Karunadasa, *ACS Cent. Sci.*, 2016, **2**, 201–209.
24 T. Ou, J. Yan, C. Xiao, W. Shen, C. Liu, X. Liu, Y. Han, Y. Ma and C. Gao, *Nanoscale*, 2016, **8**, 11426–11431.
25 M. Szafrański and A. Katrusiak, *J. Phys. Chem. Lett.*, 2016, **7**, 3458–3466.
26 S. Jiang, Y. Fang, R. Li, H. Xiao, J. Crowley, C. Wang, T. J. White, W. A. Goddard, Z. Wang, T. Baikie and J. Fang, *Angew. Chem., Int. Ed.*, 2016, **55**, 6540–6544.
27 Y. Wang, X. Lü, W. Yang, T. Wen, L. Yang, X. Ren, L. Wang, Z. Lin and Y. Zhao, *J. Am. Chem. Soc.*, 2015, **137**, 11144–11149.
28 L. Zhang, Q. Zeng and K. Wang, *J. Phys. Chem. Lett.*, 2017, **8**, 3752–3758.
29 X. Lü, Y. Wang, C. C. Stoumpos, Q. Hu, X. Guo, H. Chen, L. Yang, J. S. Smith, W. Yang, Y. Zhao, H. Xu, M. G. Kanatzidis and Q. Jia, *Adv. Mater.*, 2016, **28**, 8663–8668.
30 L. Zhang, W. Geng, C.-j. Tong, X. Chen, T. Cao and M. Chen, *Sci. Rep.*, 2018, **8**, 7760.
31 S. Bonomi, I. Tredici, B. Albini, P. Galinetto, A. Rizzo, A. Listorti, U. A. Tamburini and L. Malavasi, *Chem. Commun.*, 2018, **54**, 13212–13215.
32 G. Liu, L. Kong, P. Guo, C. C. Stoumpos, Q. Hu, Z. Liu, Z. Cai, D. J. Gosztola, H.-k. Mao, M. G. Kanatzidis and R. D. Schaller, *ACS Energy Lett.*, 2017, **2**, 2518–2524.
33 U. Schwarz, F. Wagner, K. Syassen and H. Hillebrecht, *Phys. Rev. B: Condens. Matter Mater. Phys.*, 1996, **53**, 12545–12548.
34 D. K. Seo, N. Gupta, M. H. Whangbo, H. Hillebrecht and G. Thiele, *Inorg. Chem.*, 1998, **37**, 407–410.
35 T. Krishnamoorthy, H. Ding, C. Yan, W. L. Leong, T. Baikie, Z. Zhang, M. Sherburne, S. Li, M. Asta, N. Mathews and S. G. Mhaisalkar, *J. Mater. Chem. A*, 2015, **3**, 23829–23832.
36 G. Kresse and J. Furthmüller, *Comput. Mater. Sci.*, 1996, **6**, 15–50.
37 P. E. Blöchl, *Phys. Rev. B: Condens. Matter Mater. Phys.*, 1994, **50**, 17953–17979.
38 J. P. Perdew, K. Burke and M. Ernzerhof, *Phys. Rev. Lett.*, 1996, **77**, 3865–3868.
39 J. Heyd, G. E. Scuseria and M. Ernzerhof, *J. Chem. Phys.*, 2003, **118**, 8207–8215.
40 J. Heyd, G. E. Scuseria and M. Ernzerhof, *J. Chem. Phys.*, 2006, **124**, 219906.
41 J. P. Perdew, A. Ruzsinszky, G. I. Csonka, O. A. Vydrov, G. E. Scuseria, L. A. Constantin, X. Zhou and K. Burke, *Phys. Rev. Lett.*, 2008, **100**, 136406.
42 J. Klimeš, D. R. Bowler and A. Michaelides, *Phys. Rev. B: Condens. Matter Mater. Phys.*, 2011, **83**, 195131.
43 T. Thonhauser, V. R. Cooper, S. Li, A. Puzder, P. Hyldgaard and D. C. Langreth, *Phys. Rev. B: Condens. Matter Mater. Phys.*, 2007, **76**, 125112.
44 C. C. Stoumpos, L. Frazer, D. J. Clark, Y. S. Kim, S. H. Rhim, A. J. Freeman, J. B. Ketterson, J. I. Jang and M. G. Kanatzidis, *J. Am. Chem. Soc.*, 2015, **137**, 6804–6819.
45 X. Lu, Z. Zhao, K. Li, Z. Han, S. Wei, C. Guo, S. Zhou, Z. Wu, W. Guo and C.-m. L. Wu, *RSC Adv.*, 2016, **6**, 86976–86981.
46 J. Qian, B. Xu and W. Tian, *Org. Electron.*, 2016, **37**, 61–73.
47 W. Shockley and H. J. Queisser, *J. Appl. Phys.*, 1961, **32**, 510–519.
48 Z. Xiao, W. Meng, J. Wang, D. B. Mitzi and Y. Yan, *Mater. Horiz.*, 2017, **4**, 206–216.
49 M. Born and K. Huang, *Dynamical Theory of Crystal Lattices*, Oxford University Press, Oxford, 1962.
50 S. Saha, T. P. Sinha and A. Mookerjee, *Phys. Rev. B: Condens. Matter Mater. Phys.*, 2000, **62**, 8828–8834.